THE ASTROPHYSICAL JOURNAL, 392:715–721, 1992 June 20


# ELEMENT ABUNDANCES AND PLASMA PROPERTIES IN A CORONAL POLAR PLUME

K. G. WIDING AND U. FELDMAN
E. O. Hulbert Center for Space Research, Naval Research Laboratory, Washington, DC 20375-5000
*Received 1991 August 6; accepted 1991 December 30*

## ABSTRACT

Element abundances have been determined in a coronal polar plume previously observed to have a low Ne/Mg abundance ratio associated with an open magnetic field. This study is based on images of the plume in Ne VI, VII, Mg VI–VIII, Na VIII, and Ca IX, X photographed between 300 and 600 Å by the NRL spectroheliograph on *Skylab*.

The density variation with height derived from Mg VIII 436.7 Å is satisfactorily fitted with a temperature of 843,000 K in hydrostatic equilibrium, close to the temperature expected in ionization equilibrium. It is also consistent with a small departure from hydrostatic equilibrium and outflow velocities in the range of 10–20 km $s^{-1}$. The electron density derived from the Mg VIII doublet ratio is $1 \times 10^9$ $cm^{-3}$. Hydrostatic temperatures derived from intensity-height gradients in plume images of other ions also correlate with the temperatures expected in ionization equilibrium.

Element abundances relative to magnesium at several altitudes were derived by combining plots of the ion differential emission measures. We find that the relative abundances of Na, Mg, and Ca in the plume are the same (within a factor of 2) as those in the photosphere, whereas the abundance of neon relative to magnesium is only 1/10 of this ratio in the photosphere. This is an extreme case of the composition bias present on a global scale in the corona and solar wind in which elements with a high first ionization potential (FIP), such as neon and oxygen, are less abundant relative to elements with low FIP (Mg, Si, Ca) than in the photosphere.

*Subject headings:* Sun: abundances — Sun: corona — ultraviolet: solar system

## 1. INTRODUCTION

Evidence for a systematic difference in composition between the corona and photosphere has been found in coronal spectroscopy (Veck & Parkinson 1981), in the solar wind (Coplan et al. 1990; Bochsler, Geiss, & Kunz 1986; Gloeckler & Geiss 1989) and in solar energetic particles (Breneman & Stone 1985), which are believed to originate in the corona. In a thorough compilation and review of all available observations Meyer (1985) showed that the composition differences followed a pattern in which the abundances of elements with a high first ionization potential (FIP) (C, N, O, Ne, and Ar), were under abundant in the corona by a factor of 3 or 4 relative to the low FIP group of elements (Mg, Si, Ca, and Fe) compared to the photosphere. The division between the high FIP group and the low FIP group was put at 10–11 eV. For the neon and argon abundances, which were at the time undetermined in the photosphere, cosmic values observed in various galactic media were assumed.

Using neon (FIP = 21.6 eV) as a proxy for the high FIP group of elements and magnesium (FIP = 7.6 eV) for the low FIP group, Widing & Feldman (1989, hereafter Paper I) surveyed the Ne/Mg abundance ratio in various solar features imaged at 2″ spatial resolution on *Skylab* spectroheliograms photographed in the 200–600 Å spectral range. This gave a more detailed picture of abundance variations in the outer solar atmosphere than a simple two-component division into photospheric and coronal abundance sets. The neon to magnesium abundance ratio was observed to range over a factor of 20 in different localized sources, depending on whether the associated magnetic field was open or closed.

In a following paper (Feldman & Widing 1990, hereafter Paper II) a small impulsive flare was analyzed as a prime example of the "neon-rich" group of events associated with compact magnetic fields. Essentially a photospheric abundance distribution was found: the Ne/Mg ratio of 3.6 and the Ar/Mg ratio of 0.15 represent the first determination of these abundance ratios in photospheric material.

In this paper we present a contrasting example from the group of features at the lower end of the range in the Ne/Mg abundance ratio, where the associated magnetic fields are open and diffuse.

Confirmation of element abundance differences depending on FIP have also been found in chromospheric spectra. Feldman, Widing, & Lund (1990) compared intensities of Si II, Si III, and Si IV lines with C II, C III, and C IV lines observed in the 1170–1710 Å region on HRTS spectra (Bartoe & Brueckner 1975). It was concluded that the Si/C abundance ratio was enhanced by a factor of 3 in the active region chromosphere surrounding the sunspot, relative to the same ratio in the sunspot which was essentially the photospheric ratio. It was further concluded that this was due to an enhancement of the silicon abundance on an absolute basis in the chromosphere.

Variations in the abundance ratio of iron to neon ranging up to a factor of seven have also been reported from observations of Fe XVII and Ne IX lines in active regions made by the FCS spectrometer on SMM (Strong, Lemen, & Linford 1991). The findings suggest a relatively dynamic picture of abundance variations in different spatial regions and on time scales as short as one hour.

An upper limit on the Ne/Mg abundance ratio in the corona has also been derived from *Skylab* slit spectra exposed 10″ to 40″ above the solar limb. From the absence of the forbidden Ne V line, expected at 1574.68 Å, compared with the observed intensity of Mg V 1324.45 Å, Doschek & Bhatia (1990) derived an abundance ratio of Ne/Mg $\leq$ 0.4.

Turning now to the subject of the present paper, polar plumes have been of interest as possible source regions of the solar wind because of their apparent open magnetic field structures. Our attention was drawn to them because such open field structures were typically found to be associated with low values of the Ne/Mg abundance ratio (Paper I). Polar plumes have been studied in white light at eclipse by Saito (1958, 1965). The relation between coronal plumes and polar surface features was examined by Newkirk & Harvey (1968). Three polar plumes were studied by Ahmad & Withbroe (1977) using *Skylab* Mg X and O VI image data. Several soft X-ray images of a polar plume obtained on *Skylab* were also analyzed by Ahmad & Webb (1978), with special reference to the solar wind. The polar plume studied in this paper, however, was not among those included in the previous two papers.

## 2. OBSERVATIONS

Figure 1 (Plate 5) shows selected images of the polar plume photographed on 1973 December 11 by the NRL S082 A spectroheliograph on *Skylab*. This was, by far, the brightest polar plume to be present on the *Skylab* S082 A spectroheliograms. For an idea of the relative brightness between this particular polar plume and other typical plumes see the Atlas of Extreme Ultraviolet Spectroheliograms From 170 to 625 Å (Vol. I, pp. 71–83) (Feldman, Purcell, & Dohne 1987). The plume was embedded within a large coronal hole over the north polar cap. In Figure 1 we note that the images formed in the higher stages of ionization, Na VIII and Mg VIII, extend to greater altitudes above the limb than those formed at lower temperatures, such as Mg VI and Ne VI. This is partly to be expected from the smaller electron density scale height at lower temperatures in hydrostatic equilibrium. But in fact the Ne VI and Mg VI images also show a fainter extension to higher altitudes above the short features at the base of the plume. The Mg IX 368.0 Å line is one of the brightest in the solar corona. The polar plume image in this line is mostly overexposed, resulting in large uncertainties in the intensity measurements. Therefore, for the rest of the paper the Mg IX image will be ignored.

In addition to the difference in height, the images of Na VIII and Mg VIII are smoother and more diffuse than Mg VI and Ne VI. The short, discrete structures visible in Mg VI and Ne VI are probably distinct from the hotter Na VIII and Mg VIII structures, and thus appear to comprise an inner cooler core at the base of the polar plume. We also note that strong images of the plume are present in Mg IX 368 Å at $T \sim 9.5 \times 10^5$ K (Arnaud & Rothenflug 1985) and in Fe IX 242 Å ($T \sim 9.0 \times 10^5$ K), but the emission from ions formed at $T > 1.0 \times 10^6$ K is weak or absent. At the same time, no ions formed at temperatures below those of Mg VI and Ne VI ($T \simeq 4.0 \times 10^5$ K) are present (this will be clear from the emission measure plots to be presented later). Most remarkable, there are no images of the plume in He II 304 Å and He I 584 Å. The polar plume thus appears to represent heating at coronal altitudes over only a limited range of temperatures ($3 \times 10^5 < T < 1 \times 10^6$ K).

## 3. INTENSITY–HEIGHT GRADIENTS

Images of the plume on the spectroheliogram were traced on a PDS microdensitometer along the direction of dispersion at about 10 different altitudes above the limb. The resulting densities were converted to absolute intensities using calibration curves constructed from additional exposures of active regions photographed on the same emulsion batch and developed together.

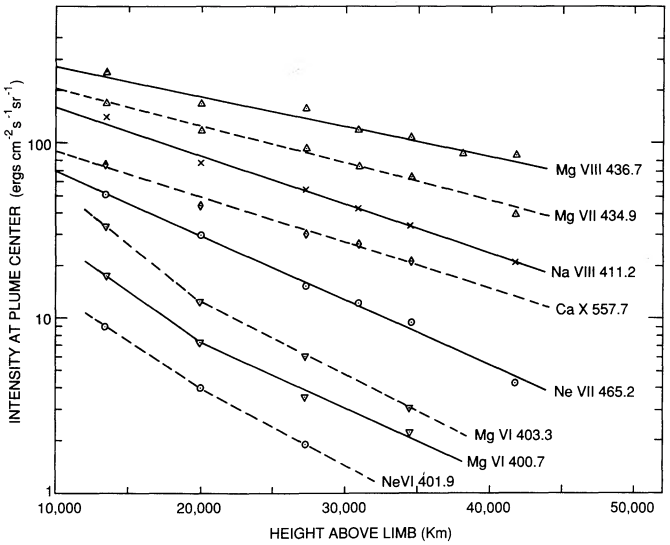


FIG. 2.—Intensities measured in various plume images as a function of height above the limb (relative intensities only—see text).

In Figure 2 the intensities measured at plume center, are plotted against altitude (relative intensities only, because some of the plots have been displaced along the intensity axis for better spacing). The data for each ion have been visually fitted with the best-fitting straight line. With the exception of Ca X the slope becomes progressively steeper between Mg VIII and the lower stage ions Mg VI and Ne VI. The ions in Figure 2 are arranged according to their peak fractional abundance calculated by Arnaud & Rothenflug (1985). However, since the distribution of emission measure in the polar plume is larger at higher temperatures, the shape of the fractional abundance distribution weighted by the emission measure needs to be taken into account. By doing so the discrepancy between Na VIII and Ca X will probably diminish or disappear.

For a preliminary discussion of these results we note that to a good approximation the intensity gradient is directly related to the density gradient which, in turn, is determined by the temperature, assuming hydrostatic equilibrium. In this approximation we obtain

$$\frac{T}{\mu} = \frac{-2.6398 \times 10^{-4}}{(\Delta \log I_0)/\Delta h}, \qquad (1)$$

where $\mu$ is the average atomic weight per particle, $I_0$ is the intensity at plume center, and $\Delta h$ is the height difference in cm. In deriving equation (1) it has been assumed that the density in the plume is constant along the line of sight, and the path length (given by the plume width) does not vary with altitude. For example, the observed slope of Mg VIII 436.7 Å entered into equation (1) yields a hydrostatic temperature of 949,000 K for $\mu = 0.615$, corresponding to a helium to hydrogen abundance ratio of 10%. This compares with a temperature of peak emission in ionization equilibrium of 810,000 K (a more refined analysis discussed below gives a Mg VIII hydrostatic temperature of 843,000 K). Similarly, the intensity gradients for the other ions in Figure 2 entered into equation (1) also give hydrostatic temperatures which are, in most cases, close to the

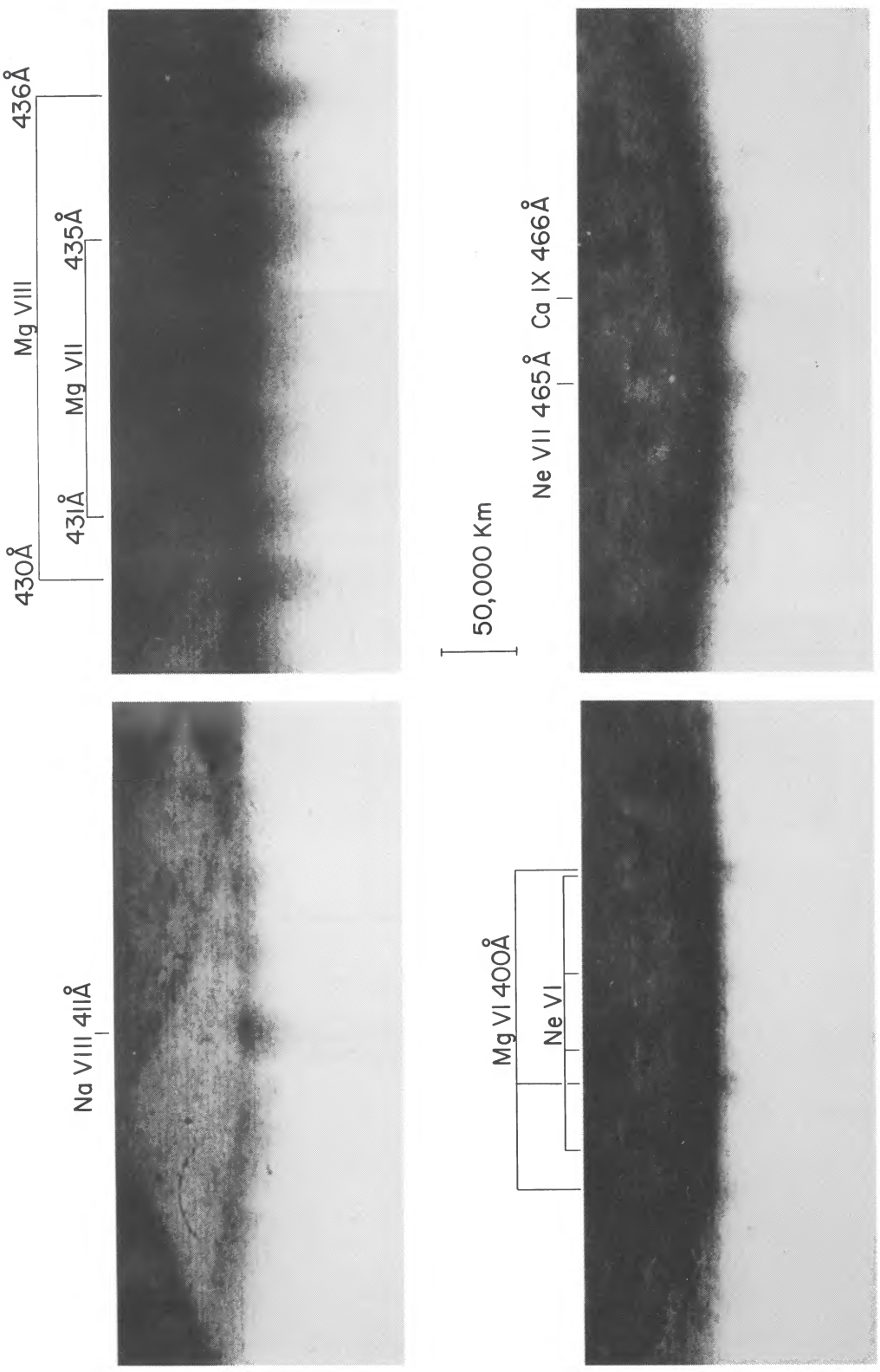


FIG. 1.—Dispersed images of a bright polar plume extending above the solar limb over the north polar cap

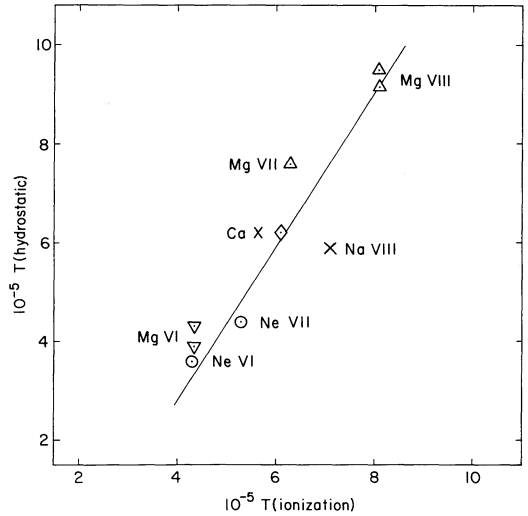


FIG. 3.—The hydrostatic temperature derived for each ion by fitting the intensity–height slope in Fig. 2 plotted against the temperature of peak emission in ionization equilibrium. Note the close relation between the two temperatures.

temperatures of peak emission in ionization equilibrium (Arnaud & Rothenflug 1985). This is shown in Figure 3 where the hydrostatic temperature derived for each ion is plotted against the ionization temperature. From the close relation between the two temperatures we conclude that the plume has a multithermal structure, and each ion is emitting in approximate hydrostatic and ionization equlibrium. This provides support for one of the basic assumptions in the abundance analysis, namely, that ionization equilibrium is valid.

The intensity gradients of Mg VI and perhaps of Ne VI show a break in the plot at 20,000 km. The hydrostatic temperatures adopted for Mg VI and Ne VI in Figure 3 were derived from the observed slope above 20,000 km. The steeper slopes at altitudes below 20,000 km may correspond to the short structures visible at the base of the plume in Figure 1. These could be superposed foreground or background structures at perhaps somewhat lower temperatures.

The correlation between the hydrostatic and ionization temperatures suggests—as a possible model—a collection of isothermal filaments or threadlike structures heated to different temperatures. The temperature in each filament would then determine both the ionization balance and gravitational scale height of the emission, as observed.

## 4. DENSITY ANALYSIS

In addition to the hydrostatic temperatures computed directly from the intensity gradients and equation (1), we have also done a more refined analysis of the Mg VIII 436.7 Å intensities, taking into account the density variation within the plume and the variation of the plume width with height to obtain the density gradient. We also consider a nonhydrostatic model in order to place limits on a possible outflow velocity of the plume.

The equation connecting the observed intensity with the electron density and other factors is

$$I(u \to l) = \frac{1.13 \times 10^{-22}}{\lambda(\mathrm{cm})} \left[\frac{\Omega_{iu}}{\omega_i}\right] \frac{1}{1 + \Sigma\, \mathrm{N_i/N_g}} \frac{A_{ul}}{\Sigma A} \times \frac{N(\mathrm{element})}{N(\mathrm{H})} \int G(T) N_e^2\, ds \ \mathrm{ergs\ cm^{-2}\ s^{-1}\ sr^{-1}}. \quad (2)$$

where $u$ and $l$ denote the upper and lower levels of the transition, $\lambda$ denotes the wavelength, $\Omega_{iu}$ denotes the collision strength, $\omega_i$ denotes the statistical weight, and $A_{ul}$ is the spontaneous decay rate. Also, $N$(element) is the element number density and

$$G(T) = N(\mathrm{ion})/N(\mathrm{element}) \exp(-\Delta E/KT) T^{-1/2}.$$

Taking an average value of $G(T)$ from behind the integral sign and collecting the other numerical factors into the quantity $A$ we rewrite equation (2) as

$$I(u \to l) = A\langle G(T)\rangle N(\mathrm{Mg})/N(\mathrm{H}) \int N_e^2\, ds. \quad (3)$$

Following the analysis of Ahmad & Withbroe (1977), we assume a cylindrical model for the plume in which the electron density decreases exponentially with radial distance from the axis of the cylinder,

$$N_e(h, r) = N_0(h) \exp - (r/\beta)^2, \quad (4)$$

where $N_0(h)$ is the density at the axis at a height $h$ above the solar limb and $\beta$ is the Gaussian width of the plume. Then the intensity profile across the plume is given by

$$I(h, \rho) = I(h, 0) \exp - 2(\rho/\beta)^2, \quad (5)$$

where $\rho$ is the projected distance from the axis and $I(h, 0)$ is the intensity at the center of the plume. Also, the emission measure at the center of the plume is

$$\int_{-\infty}^{\infty} N_e^2\, ds = (\pi/2)^{1/2} \beta N_0^2. \quad (6)$$

Inserting this expression in equation (3) we obtain

$$\frac{N(\mathrm{Mg})}{N(\mathrm{H})} N_0^2 = \frac{I(h, 0)}{(\pi/2)^{1/2} A\langle G(T)\rangle \beta}. \quad (7)$$

For Mg VIII 436.7 Å we adopted $\langle G(T)\rangle = 2.31 \times 10^{-4}$; other numerical factors appearing in the quantity $A$ are tabulated in Table 1. The plume-width parameter $\beta$ was obtained by fitting equation (5) to the intensity profile of the plume observed at several altitudes. Values of $\beta$ showed a small increase with altitude ranging from $\beta = 18{,}900$ km at an altitude of 13,400 km to $\beta = 21{,}500$ km at an altitude of 41,700 km. These widths are similar to those observed in the plumes studied by Ahmad & Withbroe (1977), particularly their plume NP1.

Finally, a value for the abundance ratio $N(\mathrm{Mg})/N(\mathrm{H})$ must be adopted. If this ratio in the plume is like the value in the photosphere, a value of $3.8 \times 10^{-5}$ can be used. However, to anticipate the main result of this paper, we find that in the plume the Ne/Mg abundance ratio is ten times smaller than in the photosphere. This could arise either because the Ne/H abundance ratio is reduced by a factor of 10, or Mg/H is enhanced by a factor of 10, or some other combination of the neon and magnesium abundances relative to hydrogen. On the basis of other data sets we have studied for abundances (Feldman et al. 1990) we think it is more likely that the major part of the effect is due to an enhancement of the Mg/H ratio in the plume rather than a reduction of the Ne/H ratio. This would qualitatively agree with the enhancement of the low-FIP metal abundances observed in the solar wind (Gloeckler & Geiss 1989; Coplan et al. 1990). We have therefore adopted $N(\mathrm{Mg})/N(\mathrm{H}) = 3.8 \times 10^{-4}$ to evaluate $N_0$ in equation (7), and the resulting values of $N_0$ are plotted against the altitude in Figure 4. Evaluating the temperature from the slope of the plot in Figure 4 we obtain $T = 843{,}000 \pm 40{,}000$

TABLE 1

ATOMIC DATA AND EMISSION MEASURES

| Ion | λ(Å) | Intensity (ergs cm$^{-2}$ s$^{-1}$ sr$^{-1}$) 13,400 km | 34,500 km | $\int G(T)dT$ | $\left[\frac{\Omega_{iu}}{\omega_i}\right]$ | $\frac{A_{ul}}{\Sigma A_{ul}}$ | $1 + \Sigma N_i/N_g$ | $T_{max}$ (K) | $\frac{N_{element}}{N_H}\left\langle\frac{N_e^2 ds}{dT}\right\rangle$ 13,400 km | 34,500 km |
|---|---|---|---|---|---|---|---|---|---|---|
| Ne VI | 401.94 | 35.9 | ... | 82.1 | 2.13 | 0.83[5] | 3.11[5] | $4.3 \times 10^5$ | $2.73 \times 10^{16}$ | ... |
| | 401.14 | (9.6)[a] | ... | | 1.04 | 0.64 | | | $(1.95 \times 10^{16})$[a] | ... |
| | 399.83 | 6.8 | ... | | 2.13 | 0.16[5] | | | $2.60 \times 10^{16}$ | ... |
| Ne VII | 465.20 | 127 | 23.2 | 65.9 | 2.21 | 1.00 | 1.15 | $5.3 \times 10^5$ | $4.13 \times 10^{16}$ | $7.5 \times 10^{15}$ |
| Mg VI | 403.32 bl. | 70.9[b] | 6.5[b] | 137.3 | 0.69 | 1.00 | 2.09 | $4.35 \times 10^5$ | $5.64 \times 10^{16}$ | $5.2 \times 10^{15}$ |
| | 400.68 | 46.7 | 6.0 | | 0.452 | 1.00 | | | $5.64 \times 10^{16}$ | $7.2 \times 10^{15}$ |
| | 399.27 | 37.6 | ... | | 0.240 | 1.00 | | | $8.52 \times 10^{16}$ | ... |
| Mg VII | 434.92 } 434.71 } | 168 | 63.5 | 143.3 | { 2.44 } { 1.84 } | 1.00 0.20 | 10.4 | $6.3 \times 10^5$ | $1.67 \times 10^{17}$ | $6.3 \times 10^{16}$ |
| | 431.32 } 431.20 } | 163 | 35.4 | | { 1.84 } { 1.06 } | 0.80 0.39 | | | $2.39 \times 10^{17}$ | $5.2 \times 10^{16}$ |
| Mg VIII | 436.73 } 436.67 } | 253 | 106 | 131.8 | { 0.83 } { 0.58 } | 1.00 0.14 | 2.89 | $8.1 \times 10^5$ | $2.36 \times 10^{17}$ | $9.9 \times 10^{16}$ |
| | 430.47 | 137 | 59.6 | | 0.58 | 0.86 | | | $2.30 \times 10^{17}$ | $9.9 \times 10^{16}$ |
| Na VIII | 411.17 | 81.6 | 19.7 | 71.5 | 1.84 | 1.00 | 1.13 | $7.1 \times 10^5$ | $2.55 \times 10^{16}$ | $6.2 \times 10^{15}$ |
| Ca IX | 466.23 | 58.2 | 15.5 | 26.1 | 4.15 | 1.00 | 1.03 | $5.9 \times 10^5$ | $2.28 \times 10^{16}$ | $6.1 \times 10^{15}$ |
| Ca X | 557.75 | 46.8 | (13.2) | 27.7 | 4.76 | 1.00 | 1.00 | $6.1 \times 10^5$ | $1.76 \times 10^{16}$ | $(5.0 \times 10^{15})$ |
| | 574.02 | 21.4 | ... | | 2.40 | 1.00 | | | $1.64 \times 10^{16}$ | ... |

[a] Values enclosed in parenthesis have less weight than the others.
[b] Corrected for blend with Ne VI 403.26 Å.

K, assuming $\mu = 0.615$. As mentioned previously, this is close to the temperature of peak emission (810,000 K) for Mg VIII 436.7 Å in ionization equilibrium. Concerning absolute values, the electron densities plotted in Figure 4, lie about 0.2 dex below the average densities of the three plumes analyzed by Ahmad & Withbroe (1977).

We next consider a hydrodynamic model of the polar plume. Following the analysis of Ahmad & Withbroe (1977) we write the momentum equation

$$v\frac{dv}{dR} = -\frac{kT}{\mu}\left(\frac{d\ln N_0}{dR} + \frac{d\ln T}{dR}\right) - \frac{GM}{R^2}, \quad (8)$$

and the continuity equation,

$$\frac{d\ln v}{dR} = -\frac{d\ln (N_0\beta^2)}{dR}. \quad (9)$$

Substituting equation (9) in (8), neglecting the term $d\ln T/dR$ and introducing the observed gradients of $\ln N_0$ and $\ln(N_0\beta^2)$ we obtain,

$$v^2 = 1.30313 \times 10^8 \frac{T}{\mu} - 1.78686 \times 10^{14}. \quad (10)$$

We have neglected the variation of gravity over the small height range considered and evaluated it for a height of 28,000

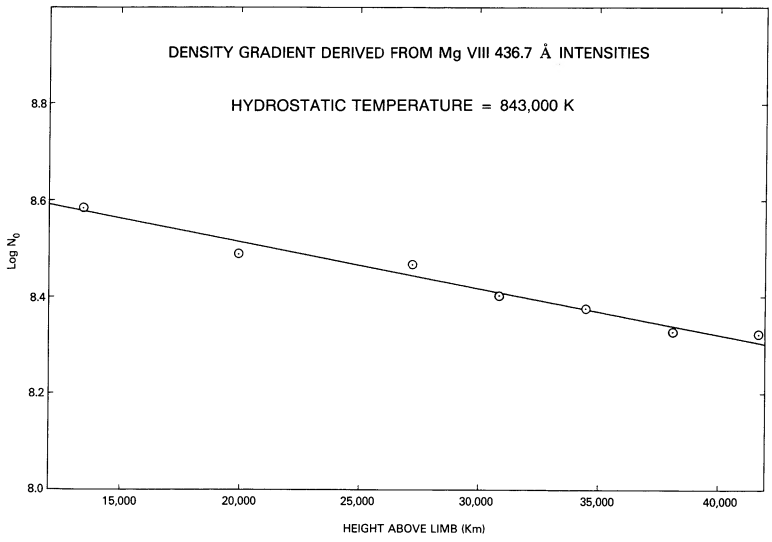


FIG. 4.—Electron density gradient and hydrostatic temperature derived from intensities of Mg VIII 436.7 Å

TABLE 2

PLUME OUTFLOW VELOCITY

| $T$ (K) | $V$ (km s$^{-1}$) |
|---|---|
| $8.43 \times 10^5$ | 0 |
| $8.50 \times 10^5$ | 11.9 |
| $8.60 \times 10^5$ | 18.8 |
| $8.75 \times 10^5$ | 25.9 |
| $9.00 \times 10^5$ | 34.7 |
| $9.50 \times 10^5$ | 47.6 |
| $1.00 \times 10^6$ | 57.6 |

km. If the He/H ratio in the plume is 0.097 (Anders & Grevesse 1989) then $\mu = 0.615$, but if He/H is 0.04–0.05, as in the solar wind, then $\mu \simeq 0.553$ and the temperature in hydrostatic equilibrium from equation (10) becomes 758,000 K. For either choice of $\mu$ the velocity variation as a function of temperature computed from equation (10) is qualitatively similar, so this variation is illustrated in Table 2 for $\mu = 0.615$, as in the previous sections.

We note from Table 2 that the outflow velocity is fairly sensitive to temperature increases above the hydrostatic kinetic temperature. To set a limit on the outflow velocity we need to estimate a limit on the temperature in the Mg VIII emission region, assuming it is emitted in ionization equilibrium. The observation of peak emission in Fe IX ($T = 9 \times 10^5$ K) and Mg IX ($9.5 \times 10^5$ K), with weak or absent emission in the higher ionization stages of these elements, suggests that the emission measure of the plume peaks in the temperature range 9.0 to $9.5 \times 10^6$ K and falls off sharply thereafter. A trial calculation using the $G(T)$ function for Mg VIII 436.7 Å and a plausible extension of the emission measure plot in Figure 5 indicates that the weighted emission of Mg VIII is shifted at most only 10,000–20,000 K higher. From this result and Table 2 we conclude that outflow velocities in the plume are likely to be only in the range of 10–20 km s$^{-1}$ with velocities in excess of 35 km s$^{-1}$ very unlikely. Qualitatively similar results were obtained from the study of three polar plumes by Ahmad & Withbroe (1977). Ahmad & Webb (1978) however, concluded that their analysis of the soft X-ray images of a polar plume were inconsistent with hydrostatic equilibrium and placed a lower limit on the expansion velocity of $\geq 100$ km s$^{-1}$.

We conclude this section by noting that an independent method of obtaining the electron density is from the intensity ratio of the Mg VIII doublet:

$$[I(436.73\ \text{Å}) + I(436.67\ \text{Å})]/I(430.47\ \text{Å}) .$$

For example, this intensity ratio is calculated to be 1.37 at $\log N_e = 8$, 1.78 at $\log N_e = 9$, and 1.90 at $\log N_e = 10$ (Flower & Nussbaumer 1975; Doschek & Feldman 1991). In Table 3 the doublet intensity ratios measured over a range of altitudes are shown, together with the corresponding electron densities derived. The scatter in the measured ratios appears to mask the small decrease in the density with altitude (Fig. 4), so we have simply adopted the average measured ratio and the corresponding electron density of $1 \times 10^9$ cm$^{-3}$. Comparison of this density with the average electron density from the Mg VIII emission measure suggests a filling factor of approximately one-third in the plume.

TABLE 3

ELECTRON DENSITIES FROM Mg VIII DOUBLET RATIO

| Height Above Limb (km) | $\left(\frac{\text{Intensity (436.73 Å)} + \text{Intensity (436.67 Å)}}{\text{Intensity (430.47 Å)}}\right)$ | $\log N_e$ |
|---|---|---|
| 13,420 | 1.85 | 9.40 |
| 19,950 | 1.60 | 8.46 |
| 30,840 | 1.65 | 8.60 |
| 34,470 | 1.84 | 9.30 |
| 38,100 | 1.65 | 8.60 |
| 41,720 | 1.86 | 9.50 |
| Average | $1.74 \pm 0.11$ (rms) | $8.98^{+0.42}_{-0.45}$ |

## 5. ATOMIC DATA AND EMISSION MEASURES

Emission measures and element ion abundances were determined from scans of the plume at five different altitudes. However, as the resulting emission measure plots and relative abundances are rather similar in all cases we present detailed results for two altitudes only. With reference to Figure 1, the scan at 13,400 km gave optimum intensities for the low-altitude feature visible in Mg VI and Ne VI, but at the same time, included a high background in the region of the Mg VII and Mg VIII lines. The background on the scan at 34,500 km was cleaner, but the Ne VI intensities became too weak to use.

To determine emission measures and abundances we rewrite equaton (2) in the form using the differential emission measure [as shown, for example, in eqns. (1)–(3) in Paper I].

$$\frac{N(\text{element})}{N(\text{hydrogen})} \left\langle \frac{N_e^2\, ds}{dT} \right\rangle = Q$$

$$= \frac{0.885 \times 10^{22} I(h, 0) \lambda(\text{cm})}{[(\Omega_{iu})/(\omega_i)] \int G(T) dT} \frac{1 + \Sigma N_i/N_g}{A_{ul}/\Sigma A_{ul}} . \quad (11)$$

Here, the differential emission measure $\langle N_e^2\, ds/dT \rangle$ is averaged over the temperature range where $G(T)$ is non-negligible, and $I(h, 0)$ is the intensity at the center of the plume observed at altitude $h$. The element-to-hydrogen ratio can also be regarded as an average value taken outside the integral sign in view of the possibility of abundance gradients across the plume. We note that the Ne/Mg abundance ratio in the plume is later found to be 0.36 compared with a typical Ne/Mg ratio of 1 in the corona outside the plume (Meyer 1985), so that the maximum abundance gradient is likely to be only of order $e$. We do not treat this possibility further but simply evaluate the average $N$(element)/$N$(magnesium) abundance ratios from the intensities at the center of the plume. Observed intensities for the ions to be analyzed at the two altitudes mentioned are given in Table 1 along with other quantities needed in equation (11). In keeping with the results of the density analysis, the ion level populations were evaluated for an adopted electron density of $1 \times 10^9$ cm$^{-3}$. The resulting values of the differential emission measure times the element abundance ratio to hydrogen are tabulated separately for the two altitudes in Table 1.

## 6. DETERMINATION OF ABUNDANCES RELATIVE TO MAGNESIUM

Relative abundances in the polar plume were determined using the same method described in Papers I and II. With the present data the plots of differential emission measure are basically defined by the three magnesium ions. Mg VI, Mg VII, and

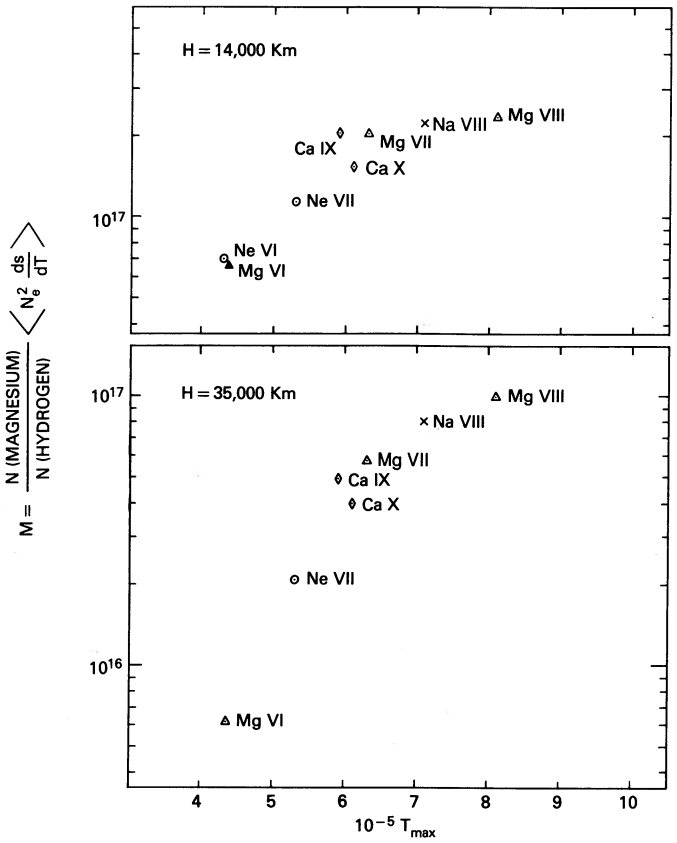


FIG. 5.—Emission measure plots at two altitudes in the polar plume

Mg VIII. For each of these ions we plot the value of $N(\text{Mg})/N(\text{H})\langle N_e^2\, ds/dT\rangle$ in Table 1 against the value of $T_{max}$, where $T_{max}$ is the temperature where the quantity $G(T) = [N(\text{ion})/N(\text{element})] \times T^{-1/2} \times \exp - \Delta E/kT$ is a maximum. This can be done because the plume has a multithermal structure, and we expect the quantity $\langle N_e^2\, ds/dT\rangle$ to be a smooth function of temperature. For ions of other elements we can obtain a corresponding value of $N(\text{Mg})/N(\text{H})\langle N_e^2\, ds/dT\rangle$ by writing

$$\frac{N(\text{element})}{N(\text{H})}\left\langle \frac{N_e^2\, ds}{dT}\right\rangle = \frac{N(\text{element})}{N(\text{Mg})}\frac{N(\text{Mg})}{N(\text{H})}\left\langle \frac{N_e^2\, ds}{dT}\right\rangle, \quad (12)$$

and finding the value of $N(\text{element})/N(\text{Mg})$ that places it on the plot defined by the magnesium ions. The resulting abundances relative to magnesium are shown in Table 4 where they are compared with relative abundances in the photosphere and in an impulsive flare (Paper II). The errors represent the range in the plume abundances found at five different altitudes, and do not take account of possible systematic errors. The final emission measure plots for the two selected altitudes are shown in Figure 5.

## 7. RESULTS AND DISCUSSION

As shown in Table 4, the Ne/Mg abundance ratio derived at two altitudes in the plume is approximately a factor of 10 smaller than the abundance ratio estimated in the photosphere, and observed in an impulsive flare—the latter believed to be a valid sample of photospheric material. At the same time, the Ca/Mg and Na/Mg abundance ratios in the plume do not differ by more than a factor of 2 from the corresponding ratios in the photosphere, and are essentially the same as in the impulsive flare.

The polar plume was one of the features included in the survey of the Ne/Mg and Ne/Ca abundance ratios in Paper I. There it was estimated that the Ne/Mg ratio in the plume was between 0.1 and 0.2. This was based on visual estimates of the relative intensities of Ne VI and Mg VI lines in the overlapping multiplets at 400 Å. The difference between the earlier estimate and the present value is the result of the intensity calibration, taking account of the atomic populations at $10^9$ cm$^{-3}$, and fitting to the emission measure plot. At the same time, a tenfold difference in the Ne/Mg ratio between the plume and photosphere remains, which we cannot account for except as the effect of real abundance changes. Of significance in this respect is the tenfold difference between the plume and flare, as this is the result of a differential comparison in which most of the calibration and atomic factors remain the same—the difference in the Ne/Mg abundance ratio depending mainly on the different relative intensities observed. This is illustrated in Figure 6 (Plate 6), where the tenfold difference in the relative abundance of neon produces gross effects in the spectra at 400 Å. In this figure the dispersed images of the flare in the bottom panel are compared with the polar plume above it. This shows that the two strongest lines of Ne VI in the flare below can barely be seen in the spectrum of the plume above.

In the survey of Paper I we saw many diffuse, open-field structures similar to the polar plume where the Ne VI/Mg VI intensity ratio at 400 Å indicated low abundances of neon relative to magnesium. At present, the Ne/Mg abundance ratio of 0.36 in the polar plume is the smallest value obtained from a differential emission measure analysis, but a preliminary analysis of another feature with diverging magnetic fields indicates a Ne/Mg abundance ratio of 0.24. It is interesting to note that Doschek & Bhatia (1990) derived an upper limit on the Ne/Mg abundance ratio from slit spectra of the corona above an active region. This was Ne/Mg $\leq$ 0.4, and was based

TABLE 4

SOLAR ABUNDANCES RELATIVE TO MAGNESIUM

| ELEMENT | POLAR PLUME 13,400 km | POLAR PLUME 34,500 km | IMPULSIVE FLARE | PHOTOSPHERE |
|---|---|---|---|---|
| Neon | 0.36 ± 0.03 | 0.36 ± 0.04 | 3.6 ± 0.3 | (3.1)[a] ± 1.3 |
| Magnesium | 1.00 | 1.00 | 1.00 ± 0.14 | 1.00 ± 0.04 |
| Calcium | 0.11 ± 0.03 | 0.12 ± 0.03 | 0.10 ± 0.04 | 0.059 ± 0.002 |
| Sodium | 0.11[5] ± 0.04 | 0.077 ± 0.03 | 0.13 ± 0.05 | 0.054 ± 0.003 |

[a] Neon abundance estimated from hot stars, H II regions, and H I gas (Meyer 1989).

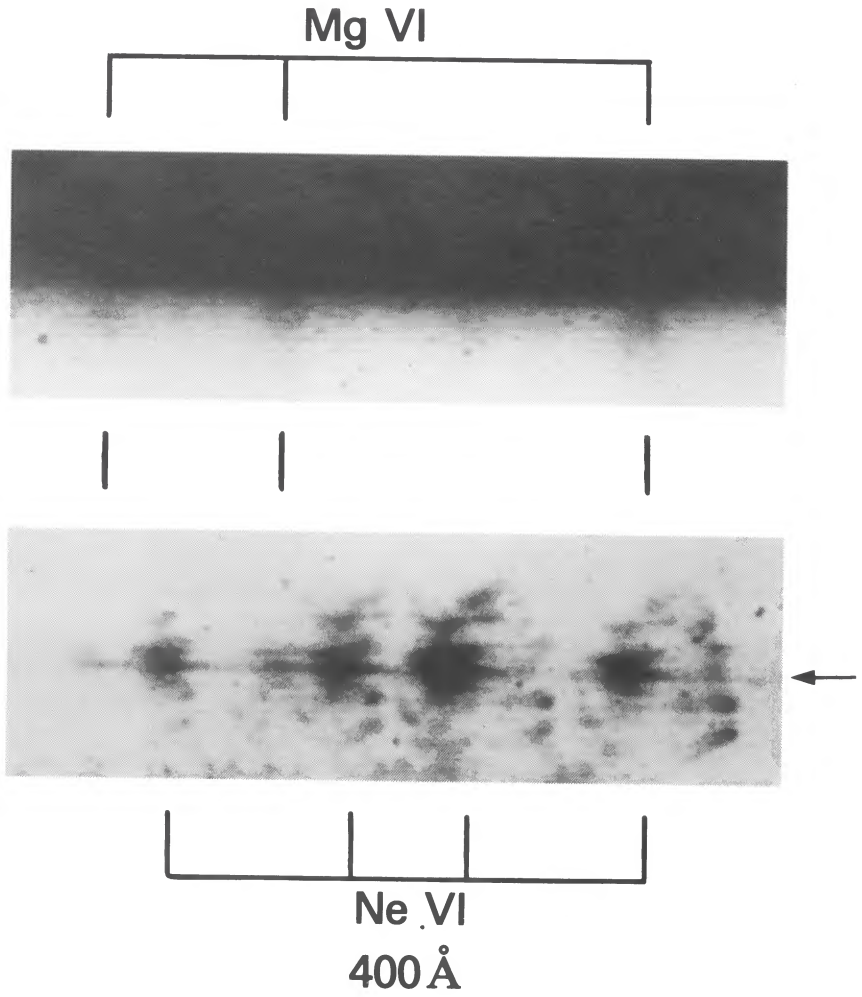


FIG. 6.—Dispersed images of the 1973 December 2 impulsive flare in the 400 Å region (*below*) compared with images of a polar plume extending above the limb (*above*). This shows the effect of a 10 × lower abundance of neon relative to magnesium in the plume. Note that the two strongest lines of Ne VI in the flare can barely be seen in the plume.

on the nonappearance of the Ne v forbidden line at 1574.68 Å compared with the Mg v forbidden line at 1324.45 Å.

The Ca/Mg ratio in both the polar plume and impulsive flare is larger by a factor of 2 than the same ratio in the photosphere (Table 4). If the FIP hypothesis is correct, there should be no change in this ratio between photosphere and corona. As discussed in Paper II, the Ca IX 466 Å line gives systematically larger values of the quantity $N(\mathrm{Ca})/N(\mathrm{H})\langle N_e^2\, ds/dT\rangle$ than the Ca X doublet lines (Table 1), which tend to give Ca/Mg abundance ratios more nearly like the photosphere. Observationally, the Ca IX 466 Å resonance line is well observed, so that the bias, if one exists, may lie in the atomic and/or ionization data for Ca IX. However, we note that coronal relative abundances of calcium determined from Ca/Fe ratios in X-ray spectroscopy of solar flares are consistently greater than the corresponding ratios in the photosphere (Doschek, Feldman, & Seely 1985; Phillips & Feldman 1991), and in solar energetic particles as well (Breneman & Stone 1985). Thus, there may yet be a real abundance difference in calcium between photosphere and corona; alternatively, the error in the photospheric abundance of calcium may be larger than the assigned uncertainty (Table 4).

We would like to thank Catherine Abbott for her help with the densitometry of the spectroheliograms.

## REFERENCES


Ahmad, I. A., & Webb, D. F. 1978, Solar Phys., 58, 323
Ahmad, I. A., & Withbroe, G. L. 1977, Solar Phys., 53, 397
Anders, E., & Grevesse, N. 1989, Geochim. Cosmochim. Acta, 53, 197
Arnaud, M., & Rothenflug, R. 1985, A&AS, 60, 425
Bartoe, J.-D. F., & Brueckner, G. E. 1975, J. Opt. Soc. Am., 65, 13
Bochsler, P., Geiss, J., & Kunz, S. 1986, Solar Phys., 103, 177
Breneman, H. H., & Stone, E. C. 1985, ApJ, 299, L57
Coplan, M. A., Ogilvie, K. W., Bochsler, P., & Geiss, J. 1990, Solar Phys., 128, 195
Doschek, G. A., & Bhatia, A. K. 1990, ApJ, 358, 338
Doschek, G. A., & Feldman, U. 1991, private communication
Doschek, G. A., Feldman, U., & Seely, J. F. 1985, MNRAS, 217, 317
Feldman, U., Purcell, J. D., & Dohne, B. C. 1987, An Atlas of Extreme Ultraviolet Spectroheliograms from 170 to 625 Å, NRL Rep. 90-4100 and 91-4100 (Washington, DC: NRL)
Feldman, U., & Widing, K. G. 1990, ApJ, 363, 292 (Paper II)
Feldman, U., Widing, K. G., & Lund, P. A. 1990, ApJ, 364, L21
Flower, D. R., & Nussbaumer, H. 1975, A&AS, 45, 145
Gloeckler, G., & Geiss, J. 1989, in AIP Conf. Proc. No. 183, Cosmic Abundances of Matter, ed. C. J. Waddington (New York: AIP), 49
Meyer, J.-P. 1985, ApJS, 57, 173
———. 1989, in AIP Conf. Proc. No. 183, Cosmic Abundances of Matter, ed. C. J. Waddington (New York: AIP), 245
Newkirk, G. A., & Harvey, J. W. 1968, Solar Phys. 3, 321
Phillips, K. J. H., & Feldman, U. 1991, ApJ, 379, 401
Saito, K. 1958, PAS J, 10, 49
———. 1965, PAS J, 17, 1
Strong, K. T., Lemen, J. R., & Linfield, G. A. 1991, Adv. Space Res., 11, 154
Veck, N. J., & Parkinson, J. H. 1981, MNRAS, 197, 41
Widing, K. G., & Feldman, U. 1989, ApJ, 344, 1046 (Paper I)